CrossMark

Gland and Zonal Segmentation of Prostate on T2W MR Images

O. Chilali[1,2] · P. Puech[1,3] · S. Lakroum[1] · M. Diaf[2] · S. Mordon[1] · N. Betrouni[1]

Abstract For many years, prostate segmentation on MR images concerned only the extraction of the entire gland. Currently, in the focal treatment era, there is a continuously increasing need for the separation of the different parts of the organ. In this paper, we propose an automatic segmentation method based on the use of T2W images and atlas images to segment the prostate and to isolate the peripheral and transition zones. The algorithm consists of two stages. First, the target image is registered with each zonal atlas image then the segmentation is obtained by the application of an evidential C-Means clustering. The method was evaluated on a representative and multi-centric image base and yielded mean Dice accuracy values of 0.81, 0.70, and 0.62 for the prostate, the transition zone, and peripheral zone, respectively.

Keywords Prostate · MR T2W images · Segmentation · Zones · Atlas

Introduction

One of the latest trends in prostate cancer management is the concept of focal therapy aiming to target only the subpart of the gland with the cancerous lesions. The development of such techniques needs a precise estimation of the cancer localizations maps. Multimodality imaging and mainly multiparametric magnetic resonance images (mpMRI) are efficient tools to this end. Computer-aided diagnosis (CAD) software solutions were widely investigated to help in images analysis. Many works focused on prostate extraction from the images and different techniques are now able to automatically segment the prostate with a sufficient accuracy [1].

On the other side, prostate is a heterogeneous organ formed by three main areas: the central area, the transition zone, and the peripheral zone [2]. The transition zone and the central zone are usually referred as the central gland. Here, we consider them as the transition zone (TZ). The peripheral zone (PZ) is the area where most prostate cancers grow [3]. Moreover, cancers of these two zones exhibit different behaviors [4]. Thus, it appears important to separate them in order to apply different analysis algorithms. However, oppositely to the gland segmentation problem, fewer studies focused on this issue. Indeed, the first study was proposed in 2011 [5]. The authors combined the mpMR images and incorporated them into a segmentation process based on the evidential C-Means classifier. Later on, other works [6, 7] introduced different techniques also based on mpMRI.

In [8–10], the authors proposed new approaches based only on the T2-weighted (T2W) MR sequence because these images are regarded as the cornerstone for prostate morphology evaluation. However, due to the lack of contrast between the two zones, the accurate segmentation of the two zones using only T2W images remains challenging. Additional information as a priori information can guide the segmentation process. In this study, starting from the initial work [5], we use the evidential C-Means classifier to segment the PZ and TZ using only the T2-weighted sequence. A priori information about the prostate morphology is modelled using an atlas [11], the

✉ N. Betrouni
nacim.betrouni@inserm.fr

1 INSERM, U1189 – ONCO-THAI – Image Assisted Laser Therapy for Oncology, University of Lille, 59000 Lille, France

2 Automatic Department, Mouloud Mammeri University, Tizi-Ouzou, Algeria

3 CHRU Lille, Radiology Department, Claude Huriez Hospital, 59000 Lille, France

ProstateAtlas (publicly available at the prostateWeb URL (http://www.medataweb.onco-thai.fr)).

Methods

The global approach is based on two major components; the first is a registration step aiming to align the target image, i.e., the image to be segmented with the atlas image while the second is a classification step aiming to drive the segmentation. Figure 1 shows the outline of the proposed method.

Registration

The registration step aims to obtain an automatic initialization. It is done using the ProstateAtlas. This atlas, described in [11], was constructed starting from 30 T2-weighted MR images. The images were selected as representative of the prostate cancer patients' population. Patients were selected in term of age, prostate volume, and prostate appearance. The result is a mean T2-weighted gray level image and a probabilistic distribution (atlas) image for each zone. These probabilistic distributions model the inter-patient variability.

The atlas mean image is registered using an affine transformation with the target T2W image, and the obtained optimal transformation is applied to the two zone atlases in order to spatially match them with the target image. This matching allows the labelling of the corresponding voxels of the target image with their corresponding probabilities to belong to each zone (class). The labelling is considered as a first solution and acts as initialization for the clustering process.

Clustering and Segmentation

Starting from the initialization obtained after the registration, this step consists in a classification process to optimize the target image voxels labelling. In order to reduce the search space, a first treatment is applied to extract the prostate from the image. As it was highlighted in the introduction, prostate segmentation from MR images was very widely discussed and different efficient algorithms were published. We applied here one of these methods which was among the first to be proposed [12]. It combines a priori knowledge of prostate shape and Markov fields modelling to guide an iterative conditional mode algorithm and to perform a Bayesian classification.

For the zonal segmentation, we chose to adapt the first applied technique based on evidence theory [5]. Evidential reasoning, also known as belief functions theory or Dempster-Shafer theory, provides an advanced modelling of fusion, conflicts between sources, and outliers.

Evidential Modelling

This modelling associates a data source or sensor S with a set of propositions, also known as the "frame of discernment." In a classification context, the frame of discernment Ω is the classes set ω_i, $\Omega = \{\omega_1, .., \omega_k\}$. If we define $P = \{P_1, .., P_N\}$ as the set of patterns/objects to be assigned to one of the

Fig. 1 Block diagram of the proposed prostate zonal segmentation method
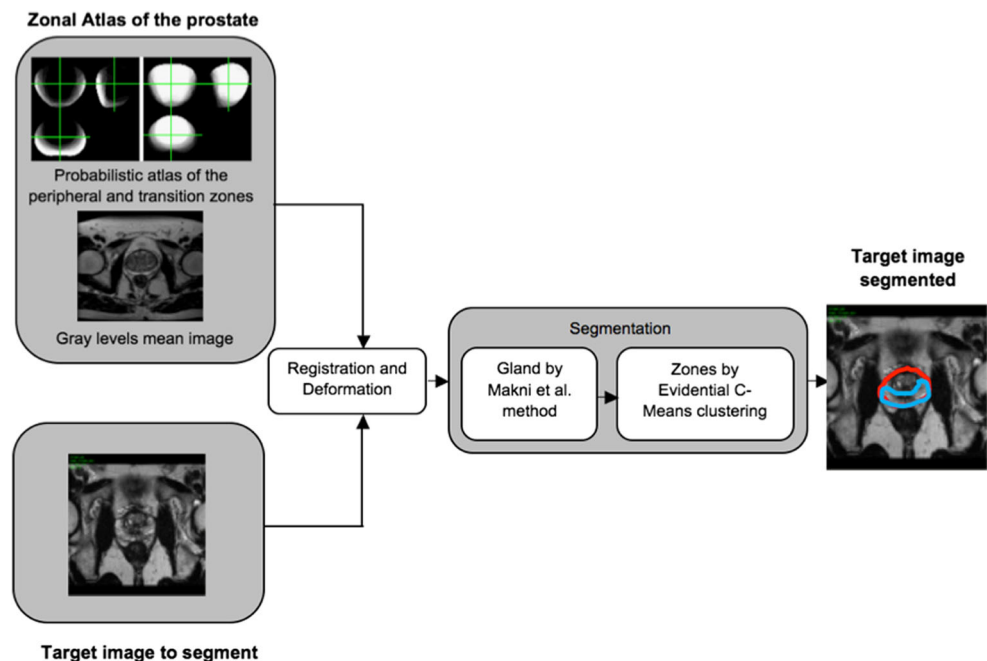
classes of Ω, then evidential reasoning allows to extract a partial knowledge on this assignment, called "basic belief assignment" (bba). A bba is a function that takes values in the range [0, 1]. For each pattern $P_i \in P$, a bba, that we note m_i, allows to measure its assignment to each subset A of Ω such as:

$$\sum_{A \subseteq \Omega} m_i(A) = 1 \tag{1}$$

The higher the value of $m_i(A)$, the stronger the belief on assigning P_i to A. Compared to the fuzzy sets model, the evidential reasoning is then capable of extending the concept of partial membership by assigning belief not only to classes but also to unions (disjunctions) of classes.

Using this model, Denoeux and Masson [13] introduced a new kind of data partition called the "Credal partition." This partition could be seen as an extension of the fuzzy partitions with bbas replacing fuzzy membership functions. Later on, the authors proposed an evidential version of the C-Means classifier that uses a credal partition. This evidential classifier, inspired by the fuzzy C-Means (FCM), is called evidential C-Means (ECM) [14]. Its principle is to classify the N patterns into k classes of Ω based on classes' centers and the minimization of a cost function. As for fuzzy partitions in FCM, a credal partition, in which each line is a bba m_i associated to a pattern P_i, is optimized in an iterative process.

From Classification to Segmentation

In the current application, each pattern is a voxel from the MR T2-weighted image. The classification process classifies the patterns into two classes: ω_1 for the peripheral zone and ω_2 for the transition zone. For each pattern, a bba measures the amount of belief assigned to:

- class ω_1: the pattern is a voxel from the PZ
- class ω_2: the pattern is a voxel from the TZ
- the set $\{\omega_1, \omega_2\}$ all hypotheses hold: the pattern may be a voxel from PZ or TZ
- the empty set ϕ: pattern is considered as outlier and rejected

The ECM model extracts and optimizes partial knowledge on patterns' assignment. A direct use of the ECM would classify voxels as independent data objects. However, voxels neighborhood, as defined by a connexity system, brings valuable information. We assume that in a homogeneous region or class, a bba is a knowledge not only on a pattern but also on its connected neighbors. Corrupted information, extracted from outliers/noise patterns, can be relaxed by information from its neighbors, which is one of the principles of noise-reducing methods and filters. Thus, introducing neighborhood

information in the ECM modelling would assimilate the ECM classifier to a region-based segmentation process.

The bba m_i of pattern P_i (associated to voxel v_i) is relaxed by combining it with bbas from spatially connected neighbors. Spatial connection is defined by a 26-connexity system. However, the contribution of each neighbor of to this combination should be weighted by the distance that spatially separates the corresponding voxels. This is particularly relevant in case of prostate MRI, where voxels are significantly anisotropic. The further the voxel, the less it should contribute to the combination.

This combination will be used as a relaxation step that allows correcting the evidential assignment of a voxel based on information from its neighbors. We propose to introduce this relaxation into the iterative process of the ECM in the following way:

$$m_i = \frac{1}{26} \left(m_i + \sum_{j=1}^{26} m_j \cdot d_j \right) \tag{2}$$

Where d_j is the Euclidean distance between voxel v_i and its spatial neighbor v_j

At the level of bbas extraction and optimization, we measure belief on the membership of each voxel to one of the classes $\omega \in \Omega$ but we also measure belief on rejection ($\varnothing$), and disjunctions $A \subseteq \Omega$ which can be interpreted as "doubt" on the membership of the voxel. A decision still has to be made to classify the voxels to one of the classes of Ω. The decision level can be reached by transforming the bbas m_i into a probability measure. This probability is calculated as:

$$\mathrm{Prob}(w_i) = \frac{1}{1 - m_i(\phi)} \sum_{\substack{\omega \in A \\ A \subseteq \Omega}} \frac{m_i(A)}{|A|}, \quad \forall \omega_i \in \Omega \tag{3}$$

where |A| denotes the number of elements of A. We finally define the decision rule R by:

$$R(P_i, m_i) = \underset{\omega \in \Omega}{\mathrm{argmax}} \left(\mathrm{Prob}(\omega_i) \right) \tag{4}$$

Experiments and Results

For the validation of the method, two databases were considered. The first, containing images from 13 patients, was from MICCAI 2012 Challenge (PROMISE 2012) (http://promise12.grand-challenge.org/Download/showSection/data) (Table 1). The second was a multi-centric database, collected from five sites. It was composed of images from 22 patients (Table 2). As prostate appearance on the images is impacted by different parameters as the patient age and the final cancer diagnosis, images were selected in a way to be representative of the population. Thus,

Table 1 Parameters of the MICCAI challenge MR database

Patients	Voxel size (mm^3)	Image size (voxel)
1–4, 6, 7	$0.625 \times 0.625 \times 3.6$	$320 \times 320 \times 20$
5	$0.625 \times 0.625 \times 3.6$	$320 \times 320 \times 20$
8–10	$0.39 \times 0.39 \times 3.3$	$512 \times 512 \times 23$
11	$0.468 \times 0.468 \times 3.33$	$384 \times 384 \times 28$
12	$0.351 \times 0.351 \times 3.3$	$512 \times 512 \times 26$
13	$0.625 \times 0.625 \times 3.6$	$320 \times 320 \times 28$

Table 3 Overall performance results on the MICCAI database

Patient	DSC (%)	DIST (mm)
Patient 1	74.13	4.3
Patient 2	74.59	4.5
Patient 3	66.82	4.8
Patient 4	76.95	4.3
Patient 5	71.30	4.5
Patient 6	85.57	2.8
Patient 7	72.96	3.9
Patient 8	82.26	3.0
Patient 9	83.69	3.1
Patient 10	75.07	4.2
Patient 11	79.43	3.85
Patient 12	78.93	3.8
Patient 13	79.63	3.15
Mean	77.02 ± 5.26	3.8

patients were in the age range 45–68 years with a mean age of 56 , while prostate volumes were in the range 24–82 cm^3 with mean volume of 43 cm^3. For diagnosis outcome, 14 patients (63. 6 %) had been diagnosed "positive" for cancer.

Images were acquired with standard T2W sequences as proposed by the different manufacturers.

Evaluation is done by comparing the segmentation result noted V_s to a reference V_r, using the following criteria:

– Overlap ratio (OR), also known as Jaccard index, is the ratio of the intersection's volume to the union's volume (optimal value = 1):

$$OR = \frac{\left|V_r \bigcap V_s\right|}{\left|V_r \cup V_s\right|} \quad (5)$$

– Dice similarity coefficient (DSC) is a similarity measure based on the Jaccard index (optimal value = 1), defined by:

$$DSC = \frac{2.\left|V_r \bigcap V_s\right|}{\left|V_r\right| + \left|V_s\right|} \quad (6)$$

– Mean Euclidean distance (DIST) between the contours (automatic and manual) drawn on the same MR image. The center of gravity of the manual contour was chosen as a reference point. Straight-line segments intersected the two contours. The intersection points were considered to compute DIST.

The PROMISE database served to highlight the performance of the gland extraction step in the proposed method

(Table 3). The reference segmentation was available for these data.

For the second database, the obtained results were compared with manual segmentations produced by an expert radiologist (more than 15 years' experience) (Table 4).

For both patients bases, the execution time was 15 ± 5 s (mean ± SD) for the registration step and about 50 ± 5 s (mean ± SD) for the segmentation step, giving an overall execution time of less than 2 min for the whole process.

Figure 2 depicts the results for two patients from the two databases. Figure 3 shows a mutual display of the segmentation result of the patient from the PROMISE 12 database, overlaid on the central image.

Discussion

In this study, we investigated the abilities of the combination of evidential clustering and prostate zonal atlases to drive a segmentation process for separating the peripheral and the transition zones on T2-weighted MR Images. Compared to the previous published studies, the current one brings two novelties. First, it operates only on the T2-weighted sequence while the most previous methods require multiparametric data. The second consists in the introduction of probabilistic

Table 2 Parameters of the multi-centric MR database

Patients	Device	Voxel size (mm^3)	Image size (voxel)
1–4, 6–15	Philips 1.5T	$0.31 \times 0.31 \times 4$	$512 \times 512 \times 15$
5, 17–20	Siemens 1.5T	$0.78 \times 0.78 \times 3$	$256 \times 256 \times 24$
16	GE 1.5T	$0.39 \times 0.39 \times 3$	$512 \times 512 \times 22$
21	GE 3T	$0.47 \times 0.47 \times 4$	$512 \times 512 \times 15$
22	GE 3 T	$0.74 \times 0.74 \times 4$	$512 \times 512 \times 20$

Table 4 Overall performance results for the 22 patients of database 2

|	DSC (%)	OR (%)	DIST (mm)
Prostate	81.78 ± 5.86	69.57 ± 8.14	3.00 ± 1.5
TZ	70.23 ± 12.06	64.40 ± 13.44	4.5 ± 1.8
PZ	62.00 ± 7.27	57.30 ± 11.60	5.2 ± 2.7
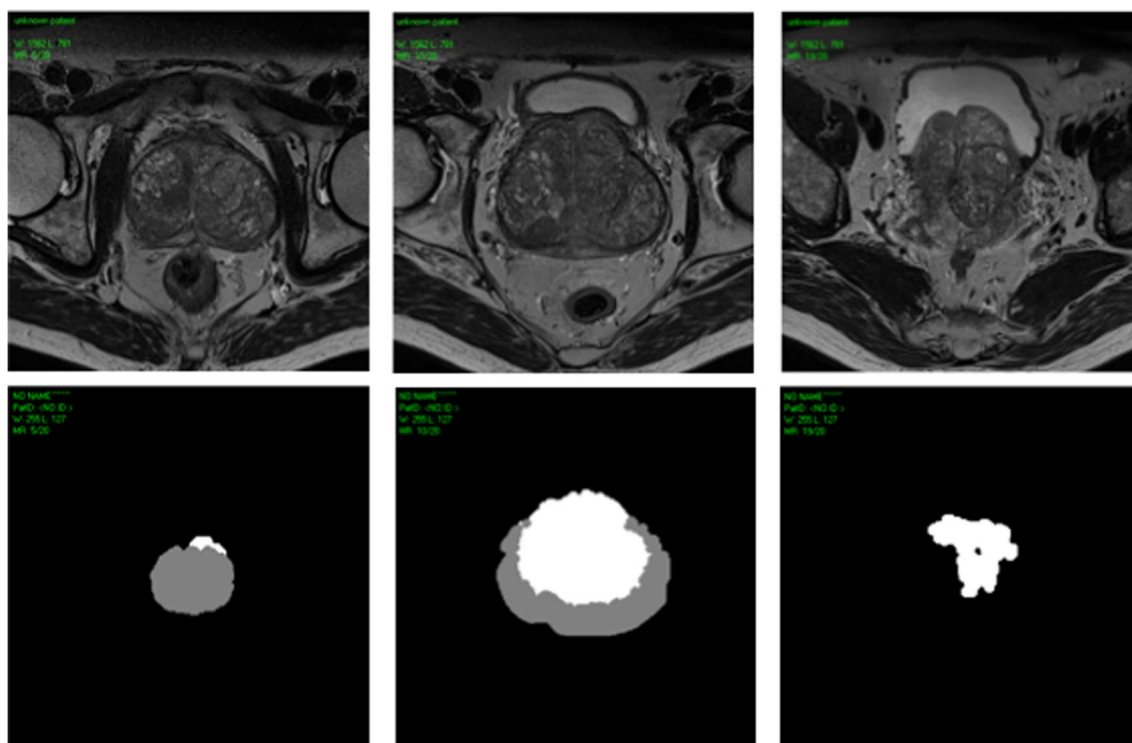
(a)
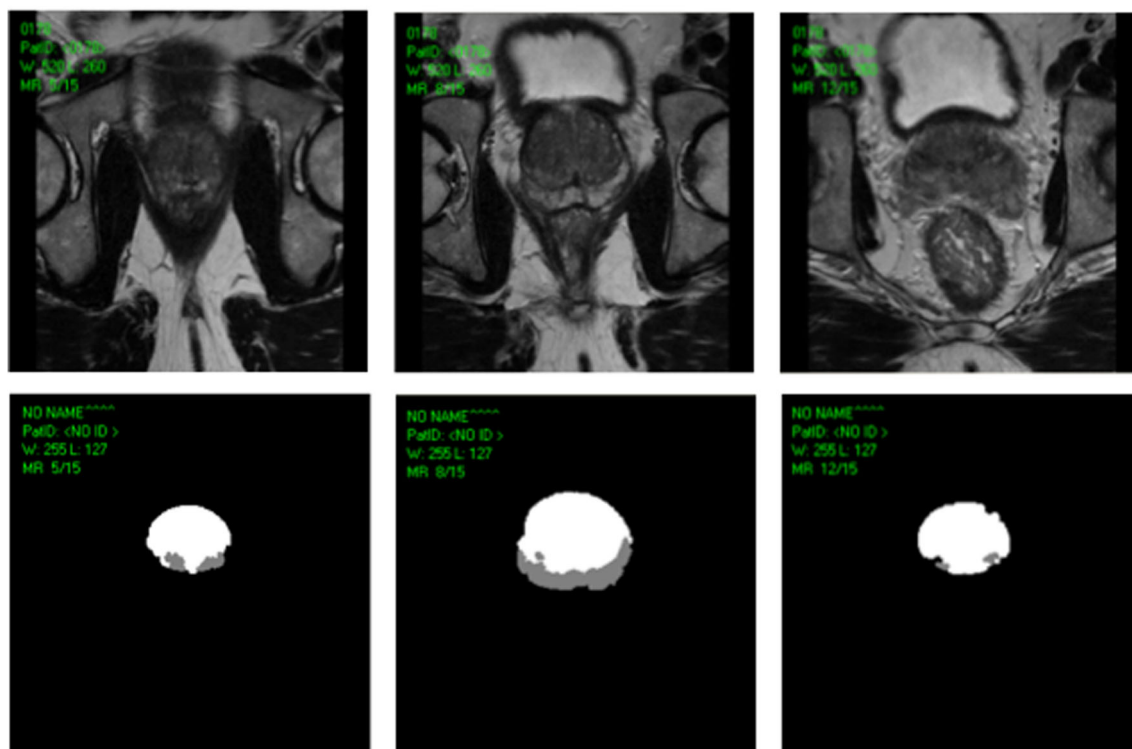
(b)

Fig. 2 Results of the two zones segmentation: the transition region (*white region*) and the peripheral region (*gray region*). From *left* to *right*: the apex, the central slice, and the base. **a** Patient 6 from the MICCAI challenge database (Prostate's DSC = 85.57 %, PZ's DSC = 51.20 %, and TZ's DSC = 74.40 %). **b** Patient 13 from the multi-centric MR database (Prostate's DSC = 88.80 %, PZ's DSC = 71.30 %, and TZ's DSC = 84.20 %)

Fig. 3 Combined display of the segmentation results overlaid on the T2-weighted image for the central slice. The first column shows the peripheral zone and the second the transition zone. Patient 6 from the MICCAI challenge database (Prostate's DSC = 85.57 %, PZ's DSC = 51.20 %, and TZ's DSC = 74.40 %).
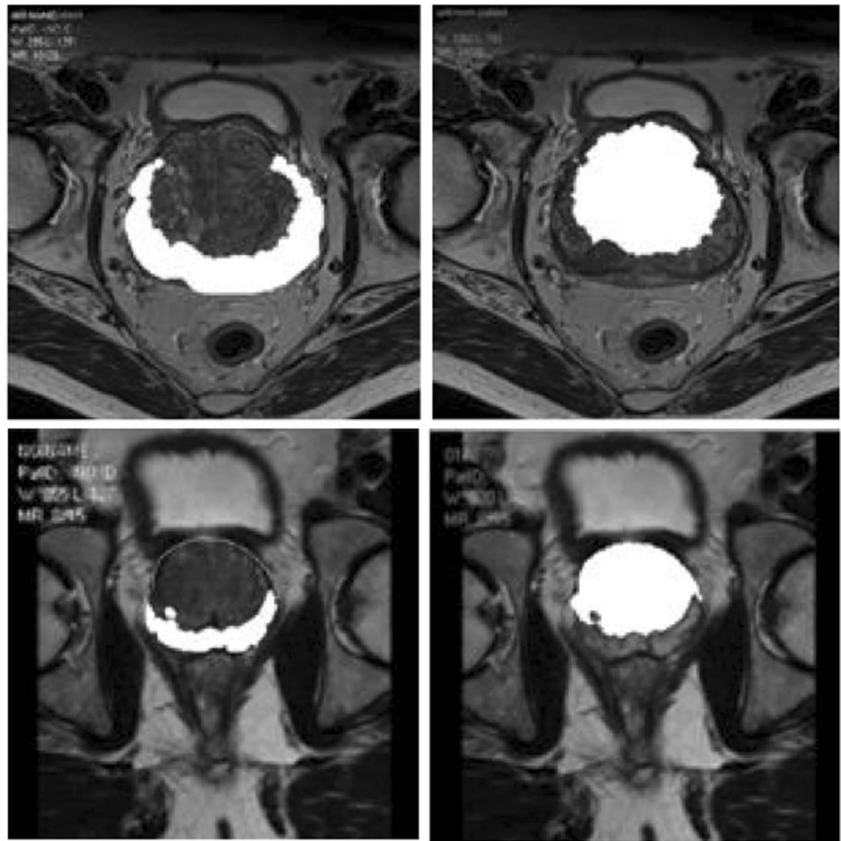
atlases of the two zones. This approach was inspired by the techniques used for gray and white matters segmentation on brain MR imaging.

The first step of the method involves a gland extraction where we have applied the method described in [12]. When applied on the PROMISE 12 challenge data, the method exhibits performances (Table 3, mean DSC = 77 %) within the range of the reported values (65–84 %) [1].

For the zonal segmentation, the overall results of the proposed method (Table 4) could appear insufficient mainly for the peripheral zone extraction (mean DSC 62 %). However, it must be stressed that these results were obtained on an image base that reflects the real life images: different appearances and volumes of the prostates. The algorithm results are very close to the expert contours in the central part of the gland. Nevertheless, for the prostate extremities, the base and mainly the apex, the results are poor. This is mainly due to the lack of signal and the partial volume effect. The enhancement of image qualities by the development of new image sequences and new images reconstruction algorithm will certainly improve the signal to noise ration ratio leading to an improvement of the segmentation.

Another issue that can be seen as a limit of this study is the validation using only a single expert while currently the trend is to take into account the inter-observer variability through STAPLE techniques for instance. Most often, the use of multi-observer references is done by generating a pseudo ground-truth reference taking into account all the references. This consensus reference can be seen as a mean contour that normalizes the most experienced observers' contours with those produced by the observers with limited experience. We chose to perform the validation by comparison to manual delineations done by an experienced radiologist (second author). He used multiparametric and multi-incidence MR images, with transverse, sagittal and coronal slices, to draw the contours as accurately as possible. Moreover, it is important to stress that in daily clinical practice, diagnosis, and therapies planning tasks are based on a single user.

Lastly, to conclude, the main aim of this work was to propose a simple technique, suitable to clinical conditions (mean execution time less than 2 min) to perform complete segmentation of the gland and the extraction of the peripheral and transition zones. All process is fully automatic even if in some cases, after convergence, some manual corrections are needed at the gland extremities.

References

1. Litjens G, Toth RB, van de Ven WA, Hoeks CA, Kerkstra SAB, van Ginneken RA, Vincent G: Evaluation of prostate segmentation algorithms for MRI: The PROMISE12 challenge. Med Image Anal 18:359–373, 2014

2. Yacoub JH, Verma S, Moulton JS, Eggener S, Aytekin O: Imaging-guided prostate biopsy: conventional and emerging techniques. RadioGraphics 32:819–837, 2012

3. Haffner J, Potiron E, Bouyé S, Puech P, Leroy X, Lemaitre L, Villers A: Peripheral zone prostate cancers: location and intraprostatic patterns of spread at histology. Prostate 69(3):276–282, 2009

4. Sakai I, Ken-ichi H, Hara I, Eto H, Miyake H: A comparison of the biological features between prostate cancers arising in the transition and peripheral zones. Br J Urol 96:528–532, 2005

5. Makni N, Iancu A, Colot O, Puech P, Mordon S, Betrouni N: Zonal segmentation of prostate using multispectral magnetic resonance images. Med Phys 38(11):6093–6105, 2011

6. Litjens G, Debats O, Van de Ven W, Karssemeijer N, Huisman H: A pattern recognition approach to zonal segmentation of the prostate on MRI, Image Computing and Computer-Assisted intervention (MICCAI). Part II. LNCS 7511:413–420, 2012

7. Maan B, Van der Heijden F, Futterer JJ: A new prostate segmentation approach using multispectral magnetic resonance imaging and a statistical pattern classifier. Proc SPIE 8314:1–9, 2012

8. Toth R, Ribault J, Gentile J, Sperling D, Madabhushi A: Simultaneous segmentation of prostatic zones using Active Appearance models with multiple coupled level sets. Comput Vis Image Underst 117:1051–1060, 2013

9. Qiu W, Yuan J, Ukwatta E, Sun Y, Rajchl M, Fenster A: Efficient 3D multi-region prostate MRI segmentation using dual optimization. IPMI 2013(LNCS 7917):304–315, 2013

10. Yuan J, Ukwatta E, Qui W, Rajchl M, Sun Y: Jointly segmenting prostate zones in 3D MRIs by globally optimized coupled level-sets. EMMCVPR LNCS 8081:12–25, 2013

11. Betrouni N, Iancu A, Puech P, Mordon S, Makni N: ProstAtlas: A digital morphologic atlas of the prostate. Eur J Radiol 81(9):1969–1975, 2012

12. Makni N, Puech P, Lopes R, Viard R, Colot O, Betrouni N: Combining a deformable model and a probabilistic framework for an automatic 3 d segmentation of prostate on MRI. Int J Comput Assist Radiol Surg 4:181–188, 2009

13. Denoeux T, Masson M-H: Evidential clustering of proximity data. IEEE Trans Syst Man Cybern 34:95–109, 2004

14. Masson M-H, Denoeux T: ECM : An evidential version of the fuzzy c-means algorithm. Pattern Recogn 41:1384–1397, 2011